Microstructure, Tensile Deformation and Fracture in Aged Ti-10V-2Fe-Al

Terlinde, Duerig, Williams

Metallurgical Transactions A
October 1983, Vol. 14A
pp. 2101-2115

1983

Microstructure, Tensile Deformation, and Fracture in Aged Ti 10V-2Fe-3Al

G. T. TERLINDE, T. W. DUERIG, and J. C. WILLIAMS

In the β-Ti alloy Ti-10V-2Fe-3Al a variety of α- and ω-aged microstructures with different yield stresses was established by combinations of forging and heat treatment. Tensile tests have shown that plastic deformation and fracture are strongly influenced by the morphology, size, and volume fraction of the different types of α-phase (primary α, secondary α, grain boundary α), as well as by the ω-phase. A detailed microscopical study revealed several deformation and fracture modes. It appears that at several sites stress and strain concentrations and subsequent void nucleation can occur and that the quantitative combinations of the different α-types determine which sites are active. The dominant deformation mode for the (α + β) solution treated and α-aged conditions was a strain localization in the α-aged matrix leading to voids at the interface between aged matrix and primary α-phase. In case of the β-solution treated and α-aged microstructures the grain boundary α leads to a strain localization in the soft α-film and to void nucleation at grain boundary triple points at low macroscopic strains. Based on the above mechanisms it is discussed in detail how varying size, volume fraction, and morphology of the α-phase affect the ductility. The embrittling effect of ω-particles can be largely reduced by a grain refinement.

I. INTRODUCTION

METASTABLE β-Ti-alloys are becoming increasingly attractive for commercial use in high strength structural components. Compared to the older α + β alloys, β-alloys exhibit higher strength to density values and good strength-toughness combinations.[1-13] Moreover, these properties can be developed in thick sections. Beside these advantages, however, several studies have shown a considerable scatter of ductilities within one structural part or forging.[7-10] These problems often arise from inhomogeneities in the microstructure which are accentuated by a strong sensitivity of the ductility to microstructure. As a result, several studies have been conducted to establish methods for controlling microstructure and for establishing the relationship between microstructure and properties. In these studies different microstructures were established by varying three factors: alloy composition, forging history, and subsequent heat treatment.[1-9] Some of the important microstructural parameters which can be controlled by combinations of the above factors are the volume fraction, distribution and morphology of the α-phase (*e.g.*, primary α, secondary α, grain boundary α), and it has been shown that they can have pronounced effects on the mechanical properties.[2-4,9] Most of the earlier studies have included only limited ranges of different microstructures. Thus, a direct comparison between the studies is difficult since usually there were differences in alloy composition, forging, and heat treating conditions, all of which contributed to different microstructures and/or strengths. This may be one of the reasons for some of the apparently conflicting results.

It, therefore, seemed appropriate to initiate a study using a fixed alloy composition in which the microstructures systematically varied over a wide range. This has been done by using combinations of forging and heat treatment.

The study described here will concentrate on the following subjects: (1) the tensile properties, especially the ductility, as a function of yield stress and microstructure; (2) the microscopic deformation (slip mode) and fracture mechanisms; (3) the correlation between the microstructures and mechanical properties.

For this study a relatively new β-Ti, Ti-10V-2Fe-3Al (Ti-10-2-3) was chosen. This alloy has the potential for extensive commercial use. Earlier studies on this alloy have been concerned with the development of chemically homogeneous material,[10] optimization of the forging conditions,[9] and elucidation of the phase transformation behavior and mechanical properties.[14] The selection of microstructures for this study will be based on results from Reference 14 and described later.

Experimental Methods

The majority of the Ti-10-2-3 alloy used in this study was supplied by TIMET (heat #P1452) as hot rolled plate. It had been thermomechanically processed starting in the β-phase field with a final α + β working operation starting from 730 °C. The β-transus was determined as 805 °C ±3 °C. The alloy contained (by weight) 10.3 pct V, 2.2 pct Fe, 3.2 pct Al, 0.15 pct O, 0.009 pct N, 0.016 pct C, and balance Ti. The other material used in this study was taken from pancake forgings which were initially worked in the β-field followed by a final upset in the (α + β) field (774 °C). The β-transus of this alloy was slightly lower than that of the plate.

Good heat treatment practice was employed to avoid atmospheric contamination. For heat treatments performed above 600 °C, specimens were wrapped in Ta foil and vacuum encapsulated. Most of the heat treatments below 600 °C were performed in a neutral liquid nitrate salt bath.

Specimens for optical microscopy were electropolished in a solution of 5 pct H_2SO_4 in methanol at room temperature

G. T. TERLINDE, Research Scientist, is with GKSS, Max-Planck-Straße, D-2054 Geesthacht, Federal Republic of Germany; T. W. DUERIG, Research Scientist, is with Raychem Corporation, 300 Constitution Drive, Menlo Park, CA 94025; and J. C. WILLIAMS is Dean of Engineering, Carnegie-Mellon University, Pittsburgh, PA 15213.

Manuscript submitted June 25, 1982.

at a voltage of 21 V. The etchant consisted of equal parts of 10 pct oxalic acid and 1 pct HF aqueous solutions.

Thin foils for transmission electron microscopy (TEM) were prepared in a twin jet electropolishing unit with an electrolyte of 59 pct methanol, 35 pct butanol, and 6 pct perchloric acid cooled to −50 °C. A voltage of 12 to 15 V was used.

For void nucleation studies fractured round tensile specimens were sectioned parallel to the tensile axis to expose the center plane, which then was electropolished. The void nucleation was investigated by SEM.

Tensile tests have been performed on electropolished and etched cylindrical specimens with a diameter of 6.4 mm and a 32 mm gage length using an Instron testing machine with a clip-on extensometer. The tests were carried out in the L-direction of the plate at a strain rate of $5.5 \times 10^{-4} s^{-1}$. The fracture surfaces of the tensile specimens have been studied by scanning electron microscopy (SEM).

II. RESULTS

Microstructure Characterization

A variety of microstructures has been chosen for this investigation based on a recent detailed study on this alloy.[14] They will be briefly introduced using a schematic phase diagram of a β-Ti alloy shown in Figure 1.

All heat treatments were performed in two steps and consisted of an elevated temperature solution treatment (ST) followed by a lower temperature aging treatment. Solution treating above the β-transus (β-ST), *e.g.*, at 850 °C, leads to recrystallized equiaxed β-phase grains. The upper optical micrograph in Figure 1 illustrates this structure. Numerous inclusions are also visible in the β-ST structure. Solution treating in the two phase ($\alpha + \beta$)-field (($\alpha + \beta$)ST), in this case between 700 °C and 780 °C, results in a β-matrix containing coarse primary α (α_p) particles. The morphology of this primary α is influenced by the forging conditions, it was equiaxed for the plate forging (lower left micrograph), and elongated (aspect ratio ~5) for the pancake forging (lower right micrograph). The volume fraction of primary α can be controlled independently of morphology by the solution treating temperature. Thus, the individual effects of α_p morphology and volume fraction on the mechanical properties can be separated. In our studies the α_p volume fraction changed from 0 vol pct at 805 °C (β-transus) to about 40 vol pct at 700 °C. Furthermore, the ($\alpha + \beta$) ST microstructures are characterized by pancake-like β-grains which contain a fine internal subgrain structure which is stabilized by the primary α.

The solution treatments were followed by aging at temperatures between 200 °C and 500 °C. Between about 200 °C and 450 °C the metastable, coherent ω-phase forms (Figure 2(a)), but it transforms after sufficiently long aging times to secondary α precipitates (α_s) (Figure 2(b)). This α forms as a uniform distribution of very small plates with a typical length of 1500 Å and a thickness of 300 Å. Above 400 °C a second type of α_s-phase forms directly in an autocatalytic manner. It has a much higher aspect ratio than the aforementioned α and is larger in size (Figure 2(c)). The conditions for formation of this α morphology include a higher aging temperature and a rapid heating rate, since heating slowly allows the ω to form first and then transform *in situ* to the fine type of secondary α. This is described in more detail elsewhere.[14] During aging, especially at

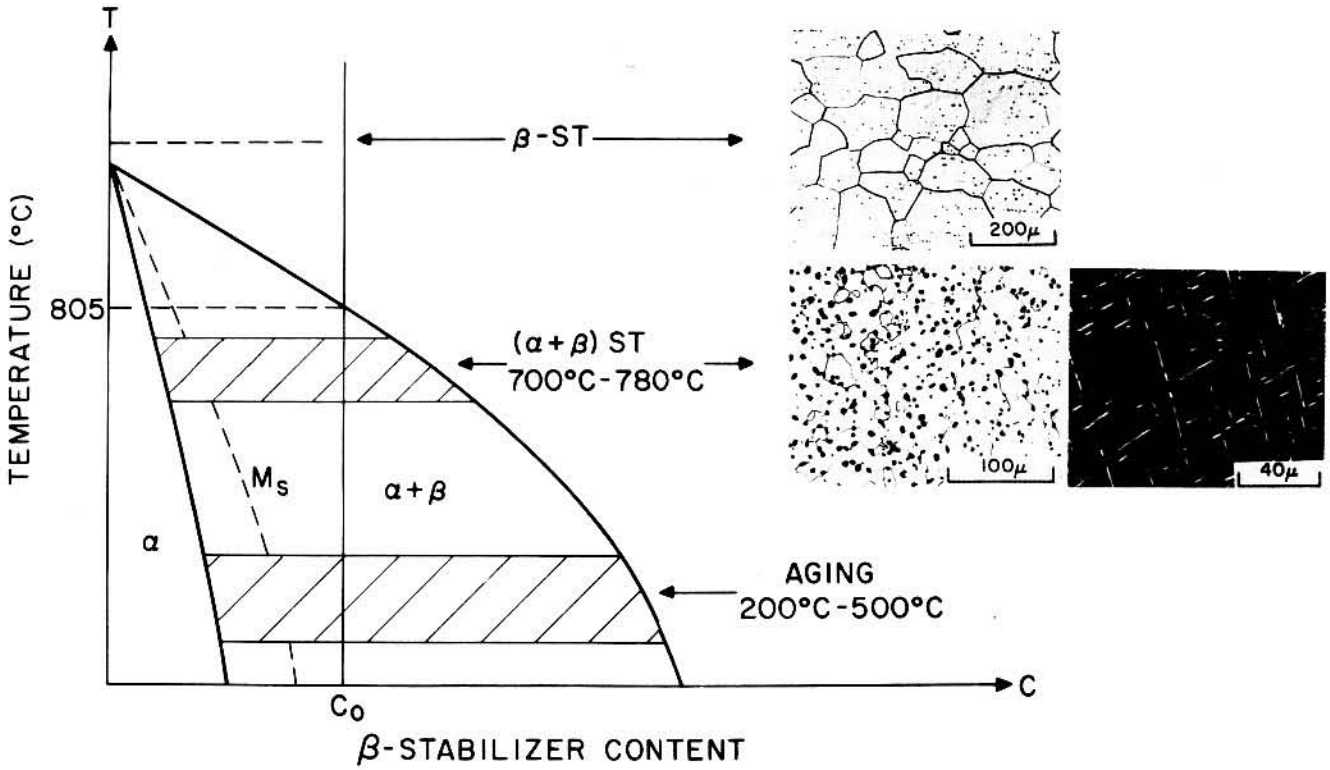

Fig. 1 — Schematic phase diagram illustrating the heat treatments and the resulting microstructures. The lower 2 microstructures show the different α_p morphologies in samples containing 10 pct α_p.

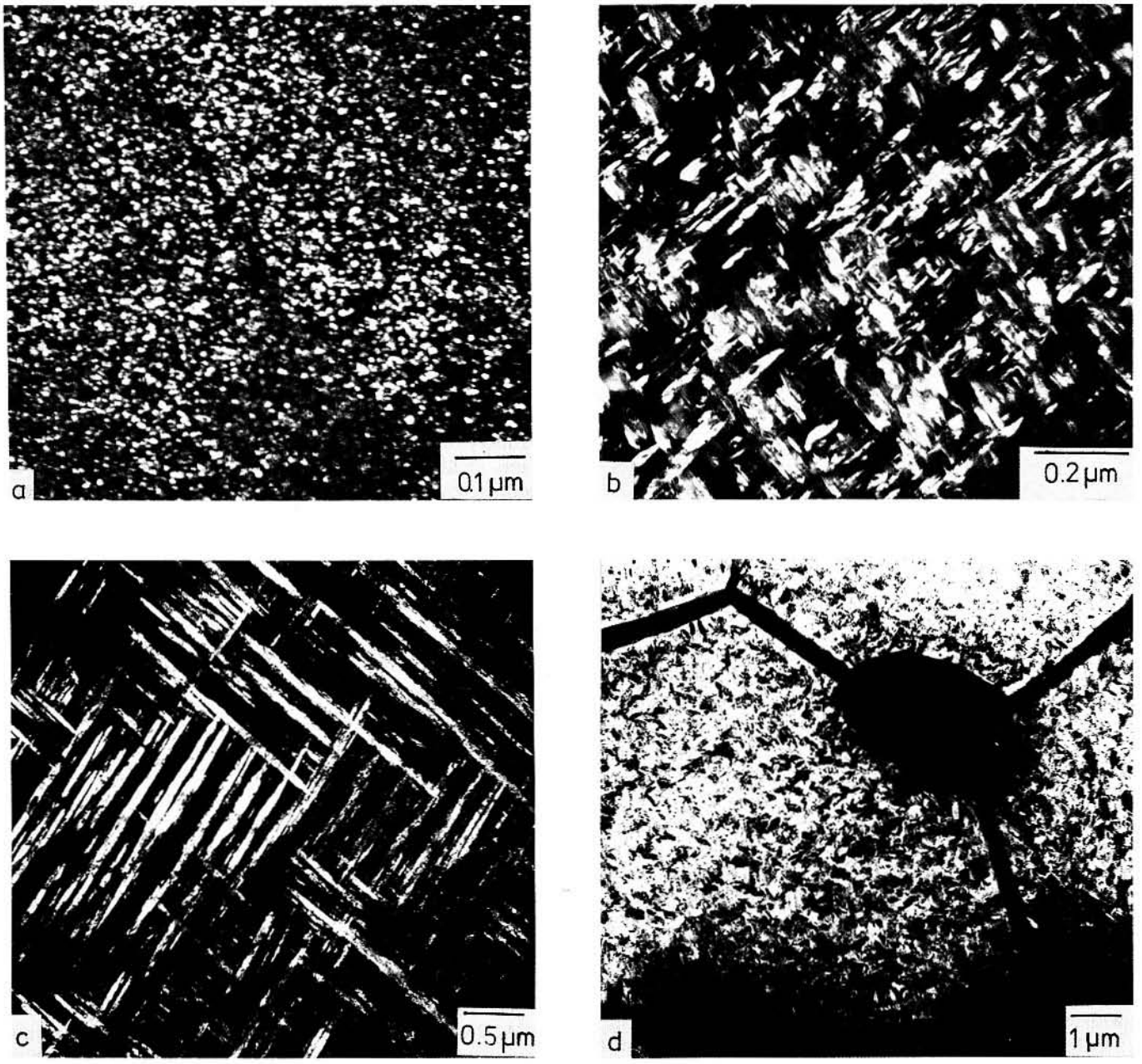

Fig. 2—Aging products: (*a*) ω-particles, TEM dark field, (*b*) α-phase formed from ω-phase, TEM dark field, (*c*) α-phase formed autocatalytically, TEM dark field, and (*d*) subgrain boundary α phase, TEM bright field.

temperatures above 400 °C, the α-phase also precipitates at grain boundaries and subgrain boundaries, and it can develop into a continuous film (Figure 2(d)).

III. TENSILE TESTS

By appropriate combinations of solution treating and aging it is possible to establish a wide range of yield stresses from about 900 MPa (130 ksi) to 1450 MPa (210 ksi) for different types of microstructures. A microstructure type is defined here as having a fixed solution treatment or volume fraction of primary α, whereas the aging condition can change.

The main interest of this study is to find a correlation between different microstructures and their strength, deformation, and fracture behavior. To do this, variations in ductility as a function of the yield stress will be presented for different types of microstructures.

In Figure 3 the yield stress, $\sigma_{0.2}$, is plotted *vs* the true fracture strain ε_F or reduction in area RA, respectively, for three α-aged microstructures and one ω-aged condition. The data in this diagram are organized according to microstructures as defined before. The α_p volume fractions chosen were 0 pct, 10 pct, and 30 pct; the aging temperatures for α-aging were between 350 °C and 500 °C and for ω-aging between 200 °C and 260 °C (details in Reference 14). The diagram shows the following results:

(1) For a constant α_p volume fraction an increase in yield stress leads to a reduction in ductility. This well-known tendency is emphasized by "trend lines" drawn in Figure 3 for each type of microstructure.

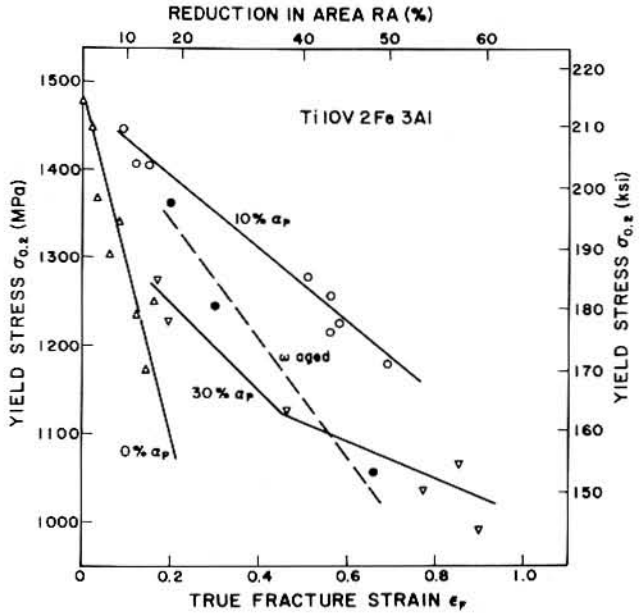

Fig. 3 — Influence of yield stress on true fracture strain for different microstructures.

(2) For the (α + β) ST and α-aged microstructures (10 pct and 30 pct α_p) an increase in α_p volume fraction reduces the ductility at all yield stress levels studied. For example, at a yield stress of about 1250 MPa (181 ksi) the microstructure with 10 pct α_p shows a true fracture strain of 0.50 compared to 0.18 for the condition with 30 pct α_p.
(3) The β-ST (0 pct α_p) and α-aged microstructures show lower ductilities than the (α + β) ST and α-aged conditions.
(4) The results of the ω-aged conditions are illustrated partially in the $\sigma_{0.2}$-ε_F diagram, Figure 3; additional data are shown in Table I. By ω-aging the β-ST condition macroscopic brittleness is found after aging to quite low apparent strengths as deduced from hardness data. The (α + β) ST microstructure with 30 pct α_p at a yield stress of 1218 MPa still shows a very low ductility (1 to 2 pct RA). In addition, however, we tested a very similar ω-aged microstructure with 30 pct α_p which was produced from a different forging, which has not been described here. After solution treatment, this forging did not have the coarse grains and substructure typical of hot rolled material, but had very small recrystallized grains of similar size as the substructure (~10 μm diameter) in the aforementioned material. This recrystallized microstructure showed a considerably higher ductility in the ω-aged condition. For example, at a strength of 1250 MPa, the true fracture strain was 0.31 (RA = 27 pct). This value is even better than the corresponding ductility of the α-aged microstructure at this yield stress. At higher yield stresses, *e.g.*, at 1350 MPa (196 ksi),

Table I. Tensile Properties of Different ω-Aged Microstructures

α_P Vol Pct	Grain/ Subgrain	Size (μm)	ω-Aging Temp. (°C)	$\sigma_{0.2}$ (MPa)	e_F (Pct)	ε_F	RA (Pct)
0	grain	≈150	260	—	0	0	0
30	subgrain	≈ 10	260	1218	0.6	0.02	2
30	grain	≈ 10	260	1245	5.3	0.31	27

Table II. Influence of α_p-Morphology on Tensile Properties for Two Different α_p-Volume Fractions at a Constant Yield Stress

α_P Vol Pct	α_P Morphology	α_s Aging Temp.	$\sigma_{0.2}$ (MPa)	ε_F	RA (Pct)
10	globular	500 °C	1250	0.50	39
10	elongated	500 °C		0.30	26
30	globular	350 °C	1250	0.20	18
30	elongated	370 °C		0.11	11

the ductility of this ω-aged microstructure is almost as good as that of the "best" α-aged condition.
(5) All the above results were received from microstructures with a globular α_p-morphology. In order to study the effect of an elongated α_p-morphology on ductility, microstructures with constant volume fractions of each α_p-morphology (10 pct, 30 pct) were aged to produce the same yield stress. The results are shown in Table II. For both α_p volume fractions investigated, the elongated morphology exhibits lower ductilities compared to the globular shape at ~1250 MPa yield stress. While the true fracture strain drops from 0.50 to 0.30 for 10 pct α_p, it is reduced from 0.20 to 0.11 for 30 pct α_p.

IV. MICROSCOPIC DEFORMATION AND FRACTURE

The microscopic details of deformation and fracture were studied mainly by SEM. In some cases the SEM observations were augmented by TEM studies. Based on preliminary studies, the various microstructures show markedly different slip modes as well as fracture behavior and are thus difficult to discuss concurrently. Therefore, this section will be divided into three parts: (a) β-ST plus α-aged, (b) (α + β) ST plus α-aged, and (c) ω-aged microstructures.

A. *β-ST Plus α-Aged Microstructures*

The β-ST plus α-aged microstructures especially in the high strength condition ($\sigma_{0.2}$ > 1300 MPa) show mainly intergranular fracture (Figure 4(b)). A surface deformation study on the gage length surface (ε = ε_F) (Figure 4(a)) reveals that the plastic deformation is very localized in the soft grain boundary α-film and leads to considerable displacements between adjacent grains. These displacements frequently have a component which is perpendicular to the specimen surface as has been determined with the aid of stereo pairs. In addition, a band of intense deformation, which starts from the grain boundary triple point and spreads into the grain interior, can be seen. It is probable that this is accommodation deformation which is necessitated by the intense localized slip in the grain boundary α film parallel to the band, and which has been stopped at the triple point. This leads to high local stress concentrations which can be relieved by accommodation slip in the adjacent grain.

At lower yield stresses the amount of intergranular fracture decreases, and instead more transgranular dimple type fracture is observed (Figure 4(c)). The dimple size is very nonuniform with sizes from less than 1 μm to about 10 μm. This could be related to the platelike shape of the secondary

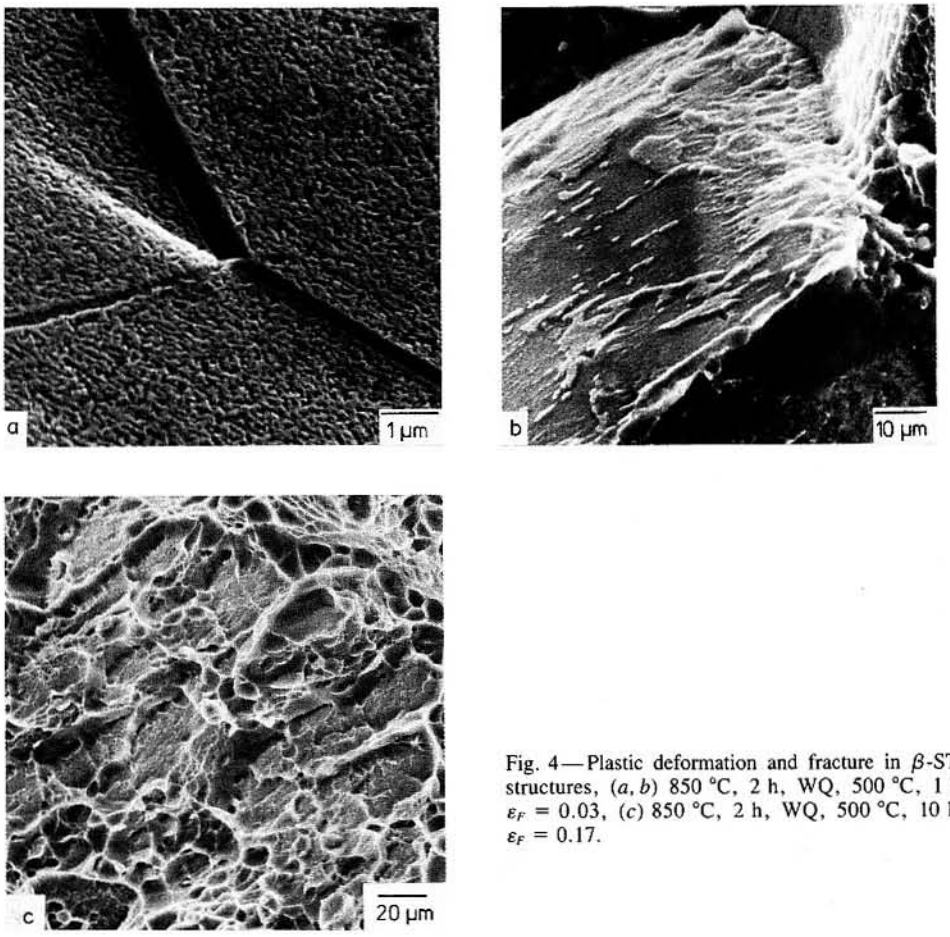

Fig. 4—Plastic deformation and fracture in β-ST plus α-aged microstructures, (*a, b*) 850 °C, 2 h, WQ, 500 °C, 1 h, $\sigma_{0.2}$ = 1367 MPa, ε_F = 0.03, (*c*) 850 °C, 2 h, WQ, 500 °C, 10 h, $\sigma_{0.2}$ = 1246 MPa, ε_F = 0.17.

α-phase (see Figure 2(c)), since depending on the orientation of the plates relative to the load axis, fracture nuclei associated with them would give very different dimple sizes.

B. *($\alpha+\beta$) ST and α-Aged Microstructures*

Typical fracture surfaces of (α + β) ST plus α-aged microstructures are shown in Figure 5. They were taken from two microstructures, one with 10 pct α_p (Figures 5(a) and (b)), the other one with 30 pct α_p (Figures 5(c) and (d)); both were aged to about 1250 MPa yield stress. Both fracture surfaces contain dimples. The dimple shape and size, however, is not very regular, and is typically larger than the α_p-spacing in those specimens. At higher magnifications there is evidence of finely spaced regions of localized plasticity which can be seen in the interior of the dimples (Figures 5(b) and (d)). These regions generally correlate in spacing with the secondary α-phase. In addition, many dimples contain what appears to be an outline of the primary α-phase. Although there is not a one-to-one correlation between the dimple size and the primary α spacing, the dimple size of the microstructure with 30 pct α_p is smaller than that with 10 pct α_p (Figures 5(a) and (c)).

In order to study the formation of such fracture surfaces, a more detailed investigation was performed starting with the microscopic plastic deformation prior to failure. Figure 6 is a SEM micrograph which shows the surface of a tensile specimen ($\sigma_{0.2}$ = 1277 MPa, 10 pct α_p) deformed to a true strain of $\varepsilon \sim 0.35$ (ε_F = 0.46). Surface steps have formed in some areas (arrows); the orientation of these steps is parallel to the secondary α plates. Apparently, the matrix has deformed plastically and the degree of deformation seems to depend on the orientation of the α_s plates relative to the loading axis. At higher strains a clear tendency for strain localization was observed. Figure 7 illustrates some details of this strain localization. The SEM micrographs were taken from regions very close to the fracture surface of a specimen which contained 10 pct α_p and was aged to $\sigma_{0.2}$ = 1250 MPa. Localized, highly deformed zones similar to the intense slip bands commonly observed in precipitation hardened alloys[15] were found. In most cases these bands occurred in only one orientation in a single β-grain, and this orientation was close to the direction of the maximum shear stress (Figure 7(a)). The bands are very long compared to the characteristic spacing of microstructural features such as α_p (Figures 7(a) and (c)). They can deviate locally, which is probably due to slightly different orientations of the subgrains. These bands are fully developed, before any void nucleation is visible (Figure 7(c)). Very close to the fracture surface a shearing process along these deformation bands starts (Figure 7(d)), which leads to a shear type fracture (Figures 7(a) and (b)), as can be seen from the elongated dimple shape. By this shearing mechanism, voids can form at the α_p particles (Figure 7(d)). Similar deformation bands can also form in the β-ST plus α-aged condition.

With increasing yield stress, the intensity of these bands increases at comparable strains; an example is shown in

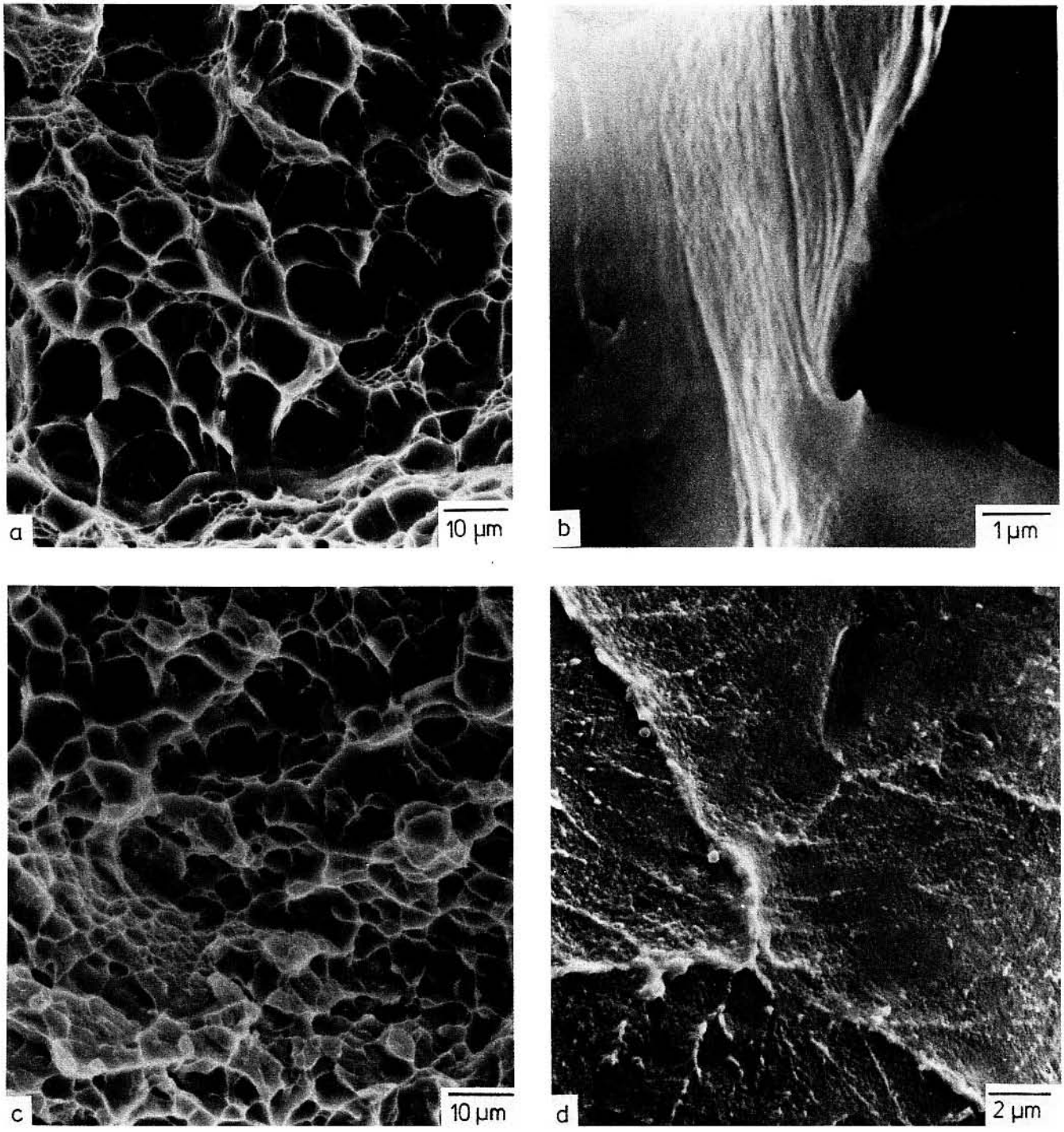

Fig. 5—Fracture surfaces of (α + β) ST plus α-aged microstructures at a yield stress of about 1250 MPa (181 ksi), SEM, (*a, b*) 10 pct α_p, (*c, d*) 30 pct α_p.

Figure 8. This SEM micrograph shows the intersection of the gage length and fracture surface of a β-ST plus α-aged microstructure which failed at a stress of 1588 MPa (230 ksi) without measurable macroscopic ductility ($\varepsilon_F = 0$). This microstructure was the only β-ST + α-aged condition examined which did not contain GBα; here the GBα probably was suppressed by the low aging temperature of 320 °C. Fracture apparently occurred along very intense localized slip bands, which are much more intense than those of the microstructure in Figure 7 with 1250 MPa yield stress. At relatively low yield stresses (~1000 MPa) the individual deformation bands are less pronounced and are much more uniformly distributed, as can be seen from Figure 9 ($\sigma_{0.2}$ = 1036 MPa, 10 pct α_p). As a result, the plastic deformation is very homogeneously distributed through the material. Here the only deformation bands which are visible are located very close to the fracture surface (Figure 9(a)), but fracture still occurs by shear (Figure 9(b)).

If the volume fraction of α_p is changed from 10 pct, as described above, to 30 pct the formation of more intense

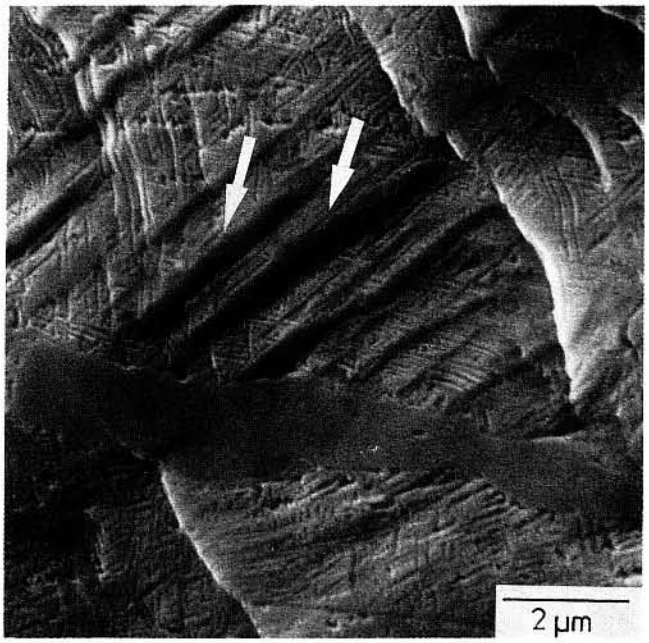

Fig. 6 — Surface deformation on an (α + β) ST plus α-aged tensile specimen at a true plastic strain of about $\varepsilon \sim 0.40$ ($\varepsilon_F = 0.46$), 10 pct α_p, aged 0.3 h at 500 °C, $\sigma_{0.2}$ = 1277 MPa, SEM.

deformation bands in the matrix is seen at comparable yield stress and plastic strain. Thus, increasing the α_p volume fraction has the same effect as increasing the yield stress. The possible reasons for this will be discussed later.

Additional evidence for the occurrence of localized deformation was found by TEM. Tensile tests were interrupted before the onset of fracture. Thin foils were prepared from the highly deformed necked regions. The following two figures show the deformation structures observed in two different specimens. Figure 10 illustrates a microstructure with 10 pct α_p whereas Figure 11 illustrates one with 30 pct α_p. Although both were α-aged to about 1250 MPa yield stress, the ductilities differed substantially (Figure 3).

Figure 10(a) shows generally uniform plastic deformation throughout the microstructure. In some areas a localized deformation is starting as illustrated in Figure 10(b), which leads to a bent shape of the secondary α plates. Trace analysis has shown that two directions in which this localized plastic deformation occurs are $\langle 110 \rangle_\beta$ and $\langle 112 \rangle_\beta$. The secondary α is also heavily deformed to a bent shape close to α_p-particles and subgrain boundaries (Figure 10(c)).

Figure 11 supports the observations of Figure 10 and provides some additional information. Figure 11(a) shows the interaction of a deformation band with a primary α particle. Apparently at least two bands (see arrows) have cut through the interface between α_p and the aged matrix causing offsets in the order of 0.1 μm. In addition, by imaging one of the bands (Figure 11(b)) it appears that the bending of the secondary α plates is more localized and more intense than in the 10 pct α_p microstructure despite the lower macroscopic strain.

In addition to the microscopic deformation, the correlation between void nucleation and strain localization has been examined. To do this, failed tensile specimens were sectioned longitudinally, and one of the flat surfaces was electropolished and etched. Void nucleation was studied below the fracture surface in the center of the specimen. Figure 12 summarizes the results. The majority of voids were associated with α_p-particles as is illustrated in Figure 12(a). Figure 12(a) also shows some evidence of the void formation process. If the voids on the lower left and upper right are connected by constructing a straight line between them, one can see that the α_p-particle in the center is sheared off along this line and starts to form a void. Therefore, together with the observations in Figure 11, it seems that deformation bands cut through the α_p-particles and start void nucleation. It is not clear exactly where the voids start, but it is most likely that they start at the interface between α_p and the aged matrix because of the high stress concentrations and strain incompatibility there.

Voids were also observed at sites where subgrain boundaries impinge on the primary α-phase (Figure 12(b)). Also, voids form at the interface between the secondary α-phase and the β-matrix (Figure 12(c)) as well as at inclusions.

Generally, all the above mentioned voids were relatively small even very close to the fracture surface and didn't show a strong tendency to coalesce to form larger cracks. One possible explanation for this observation is that once the first voids form, they grow very quickly and become unstable and that this happens only in a very small volume of the specimen.

Besides a variety of α-aged conditions, some selected ω-aged microstructures were studied. These were the β-ST and ω-aged condition ($\varepsilon_F = 0$) and the (α + β) ST plus ω-aged condition with a true fracture strain of 0.31 (see Table I). Extremely intense slip bands are observed on the gage length surface (Figure 13(a)) of the β-ST plus ω-aged condition with a β grain size of about 150 μm. These slip bands form because the coherent ω particles are sheared by moving dislocations, as has been shown previously.[15] Fracture occurs along the slip bands in a step-like pattern which is caused by concurrent shear cracks which form on several parallel slip bands and coalesce by tearing (Figure 13(b)).

The (α + β) ST plus ω-aged condition with a much smaller grain size ($\sim$10 μm) also shows slip bands developing. However, they are much less intense, are more finely spaced, and their length is smaller due to the reduced grain size (Figure 13(c)). The fracture surface shows a dimple type fracture and, at a higher magnification, traces of the slip bands are visible (Figure 13(d)). A TEM examination of a highly deformed ($\varepsilon \sim \varepsilon_F$) specimen of the above microstructure showed the existence of intense slip bands in the ω-aged matrix (Figure 14(a)). Figure 14(b) illustrates that these slip bands are strong enough to cause offsets at the grain boundary which can lead to crack nucleation at these sites. It must be kept in mind that this microstructure contains 30 pct α_p, which also can play an important role in the fracture process. However, the experimental evidence strongly suggests that the reduction in grain size is the more important factor behind the large change in ductility. This is supported by the fact that the microstructure with 30 pct α_p which had coarse grains containing a substructure instead of small recrystallized grains, showed a very poor ductility.

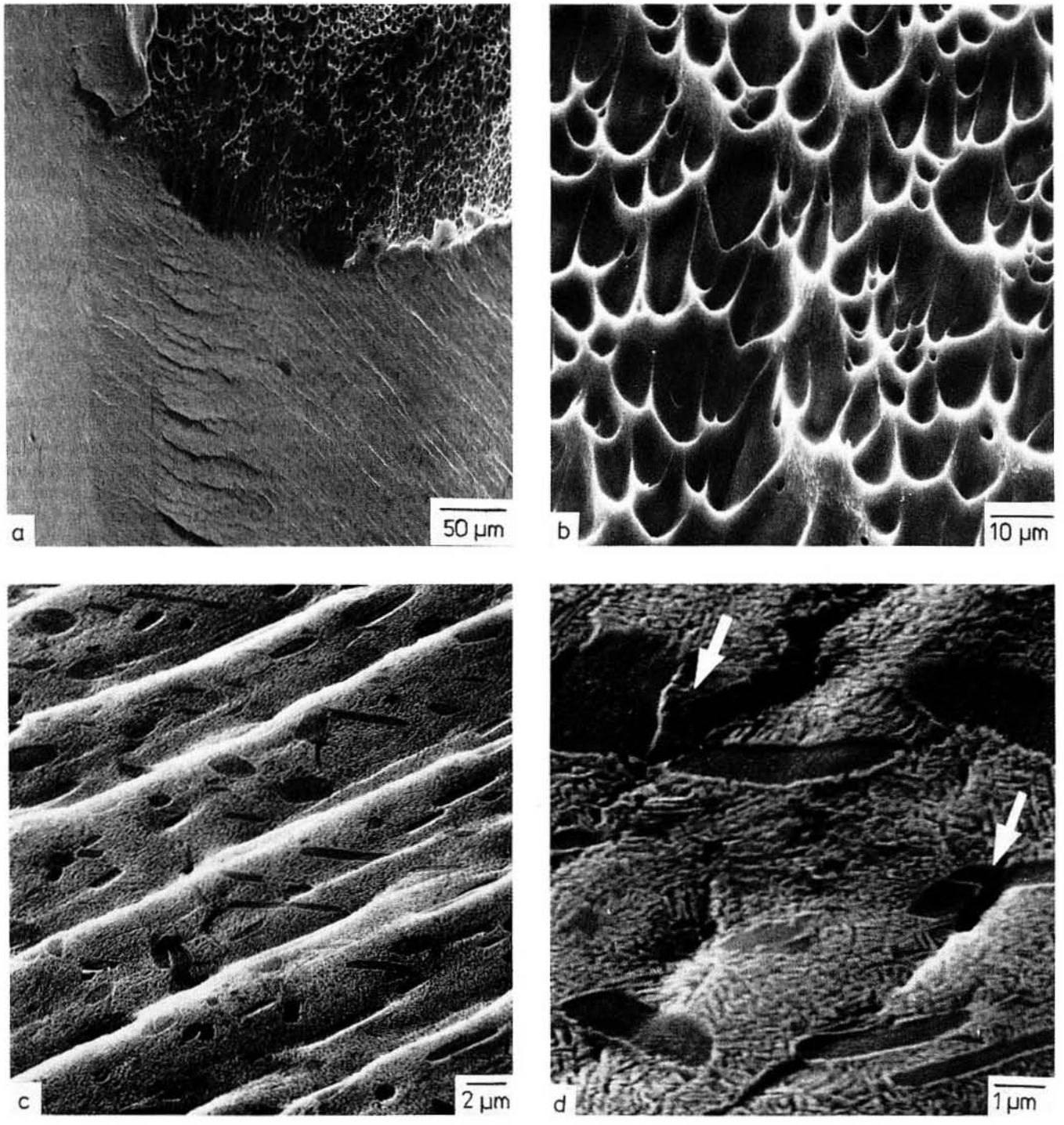

Fig. 7—Plastic deformation and fracture in an (α + β) ST plus α-aged microstructure, $\sigma_{0.2}$ = 1250 MPa. (*a*) Intersection of gage length surface and fracture surface, (*b*) fracture surface, (*c*) deformation bands at strain smaller than fracture strain, and (*d*) deformation bands at fracture strain.

V. DISCUSSION

The results have shown that, for Ti-10-2-3 with a variety of microstructures, a wide range of yield stresses can be reached and that the ductility response is strongly influenced both by the microstructure and by the yield strength.

Based on these results, the discussion will focus on the following topics: first, the mechanical properties will be discussed with emphasis on the ductility. Second, the different slip and fracture modes will be discussed and an attempt will be made to correlate the mechanical properties and microstructures on the basis of the observed slip and fracture modes.

A. *Mechanical Properties*

The ductility values of the α-aged conditions have shown a very strong sensitivity to changes in yield stress and microstructure (Figure 3, Tables I and II). From the "trend lines" in Figure 3, for example, a 100 MPa (14.5 ksi) increase in

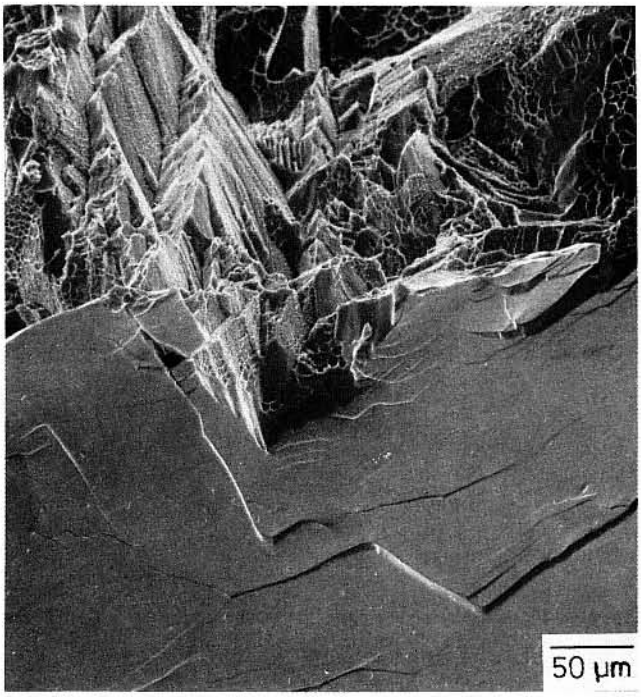

Fig. 8—Plastic deformation and fracture in a β-ST plus α-aged microstructure, no GBα, 850 °C, 2 h, WQ, 320 °C, 5 h, $\sigma_{0.2}$ = 1588 MPa (230 ksi), ε_F = 0, intersection of gage length surface and fracture surface, SEM.

yield stress can cause a reduction of the true fracture strain of $\Delta\varepsilon_F = 0.25$ (ΔRA = 23 pct) for the microstructure with 10 pct α_p. By comparison, the ductility of the β-ST plus α-aged condition (0 pct α_p) is less sensitive to variations in strength, and the equivalent decrease in fracture strain is $\Delta\varepsilon_F = 0.06$. The ductility also is very sensitive to changes in microstructure. The most pronounced effect corresponds to a change from 10 pct to 0 pct α_p, which at a yield stress of 1250 MPa reduces the ductility from $\varepsilon_F = 0.55$ (RA = 42 pct) to $\varepsilon_F = 0.15$ (RA = 14 pct). At lower yield stresses this effect is even more pronounced. These observations have important practical implications regarding the processing and heat treatment of this alloy. For example, the control of forging or heat treatment practice must be carefully monitored in order to guarantee acceptable and reproducible ductility. That is, any solution treatment close to the β-transus must be very carefully controlled since solution treatment only slightly above and below the β-transus—resulting in 0 pct α_p and 10 pct α_p, for example—leads to very different microstructures and ductilities (Figure 3). Equally important, solution treating below the β-transus at slightly different temperatures can also lead to significant ductility changes (Figure 3). In addition to solution treatment temperatures, the aging treatment also must be carefully controlled since changes in the rate of heating to the aging temperature can cause considerable differences in the nature of α_s precipitation. This also can lead to changes in the yield stress and ductility.[14]

Considerable scatter in the ductility due to chemical inhomogeneities has been reported.[10] Based on our results, this is not surprising. The chemical composition mainly determines the volume fraction of α_p after a certain solution treatment. Since local variations in the chemical composition which are equivalent to a 40 °C change of the β-transus have been observed in Ti-10-2-3,[10] the local variations in α_p-volume fractions after a solution treatment can be considerable and can lead to significantly different mechanical properties within a structural part.

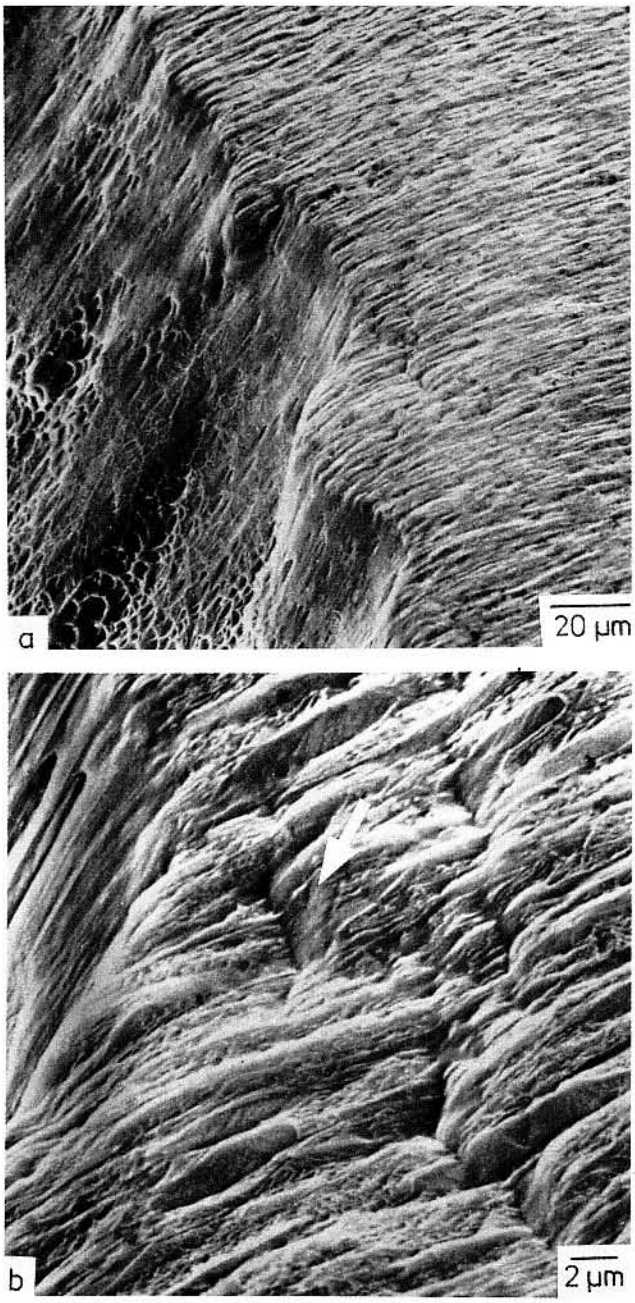

Fig. 9—Plastic deformation and fracture in an (α + β) ST plus α-aged microstructure, 15 pct α_p, aged 1 h at 650 °C, $\sigma_{0.2}$ = 1036 MPa, ε_F = 0.77, SEM.

The well-known embrittling effect of ω-particles[15] can effectively be avoided by properly reducing the β grain size (Table I). In fine grained material, the ductility of the ω-aged microstructure with the small grain size is competitive with that of the most ductile α-aged conditions, especially at high yield stresses. This ω-aged microstructure is attractive insofar as it exhibits fatigue strength values comparable to α-aged microstructures and a clear trend

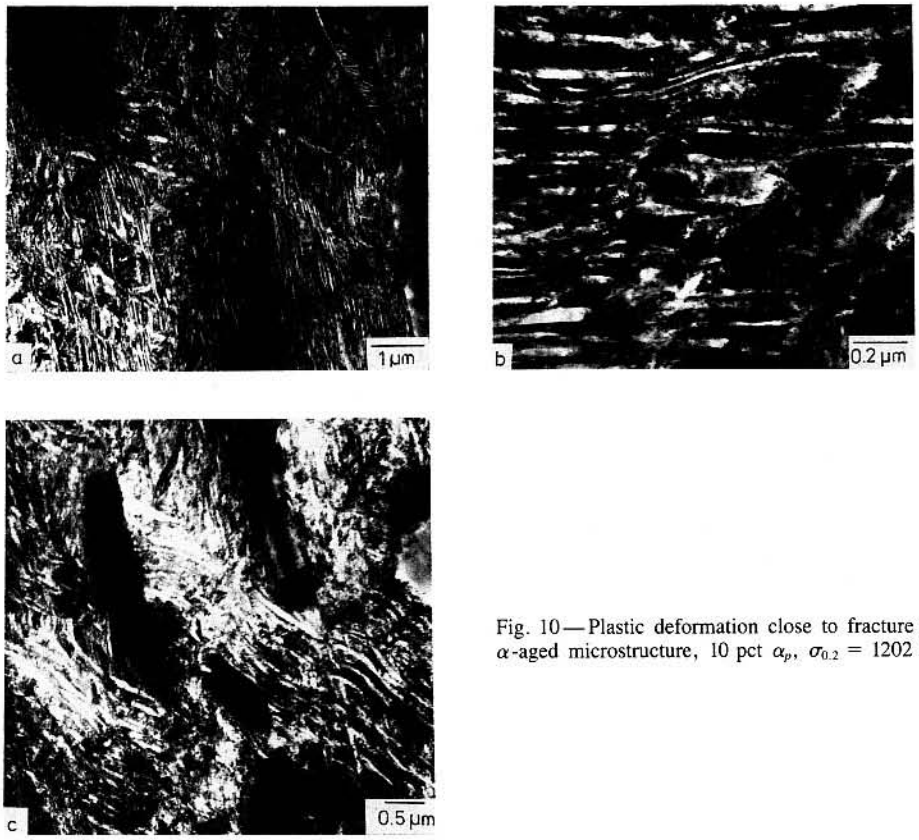

Fig. 10—Plastic deformation close to fracture in an (α + β) ST plus α-aged microstructure, 10 pct α_p, $\sigma_{0.2}$ = 1202 MPa, ε_F = 0.63, TEM.

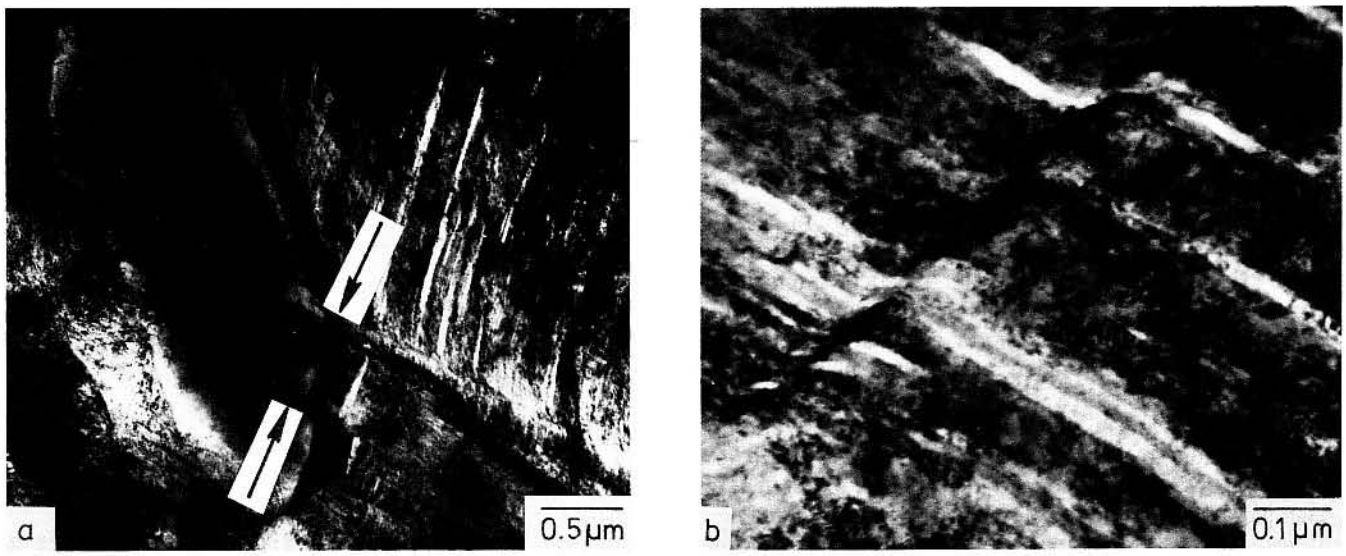

Fig. 11—Plastic deformation close to fracture in an (α + β) ST plus α-aged microstructure, 30 pct α_p, $\sigma_{0.2}$ = 1238 MPa, ε_F = 0.17, TEM.

toward higher threshold values in fatigue crack propagation, as recent studies have shown.[16,17]

B. *Microscopic Deformation, Correlation*

Before entering into a more detailed discussion of the results, it appears to be useful to point out in somewhat general terms the complex nature of plastic deformation in a two phase alloy (Figure 15) such as this. These alloys consist of a β-phase matrix which contains α-phase precipitates. Both phases are ductile and can deform plastically. From several studies there is evidence that the yield stress and subsequent strain hardening of the two phase mixture strongly depends on the size, morphology, and volume fraction of the different types of α present (α_p, α_s, GBα, SGBα).[18,20,21] Since all the α-aged conditions contain a mixture of α-types with numerous combinations of size, morphology, and volume fraction (see Figure 2), it is very

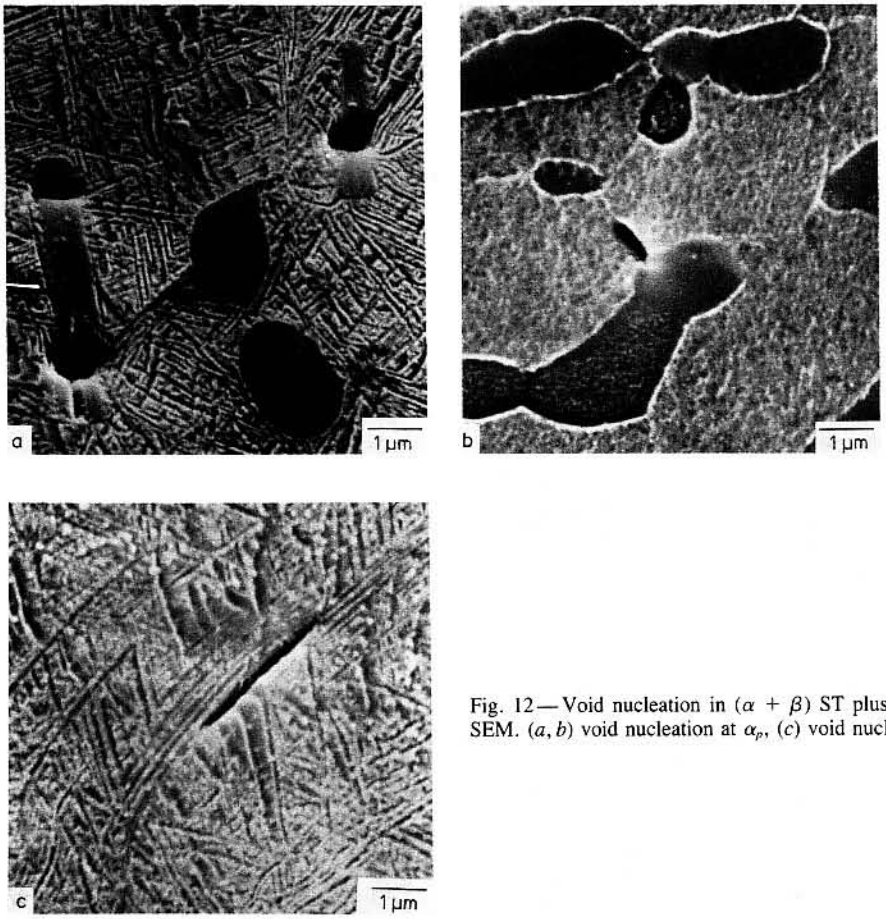

Fig. 12—Void nucleation in (α + β) ST plus α-aged microstructures, SEM. (*a*, *b*) void nucleation at α_p, (*c*) void nucleation at α_t.

difficult to separate the individual contributions of each factor to plastic deformation and fracture. Therefore, the discussion will be limited to a more qualitative explanation of the microscopic observations. For practical reasons this will be subdivided into β-ST plus α-aged, (α + β)ST plus α-aged, and ω-aged microstructures.

(1) *β-ST plus α-aged microstructures*

The predominant microstructural parameter responsible for the relatively low ductilities of this microstructural condition is the grain boundary α film (Figure 4). As has been shown here and in more detail elsewhere for similar microstructures,[2,4,14] the presence of grain boundary α leads to long soft zones which deform preferentially during plastic deformation, since the aged matrix is considerably stronger. This results in large plastic strains distributed over a relatively small volume of the material. Moreover, this occurs at stresses less than those corresponding to the yield stress of the matrix. Because of the long slip length (≤grain size) high stress concentrations and high local strains develop at grain boundary triple points, where further propagation of the slip is difficult because of the higher flow stress of the α + β matrix (Figure 15, arrow 1). This can lead to fracture at low macroscopic strains, although the local strains in the grain boundary α are high. Controlling factors for crack nucleation are the length and thickness of the soft grain boundary zones as well as the yield stress difference between the aged matrix and the soft zone.[18,19] Reducing the length of the zones, for example, by a smaller grain size has been shown to increase the ductility of an age hardened Ti-Mo alloy considerably.[18] This has been proven indirectly also in this study, since in the (α + β)ST plus α-aged conditions the subgrains or grains with a diameter in the order of 10 μm also develop an α-film during aging, but the α-film is not responsible for the main void nucleation process. Even if subboundary α were responsible for initiating fracture, in such cases much higher ductilities are reached compared to the β-ST plus α-aged conditions.

Reducing the yield stress difference between GBα and the matrix by lowering the latter has been shown to increase the ductility, too (Figure 3). This ductility increase is accompanied by an increasing amount of transgranular fracture (Figure 4(c)). This observation could be explained as follows: Beside the GB-α-film also the aged matrix deforms plastically more and more, and before crack nucleation occurs at the grain boundaries, the matrix itself develops deformation bands starting, for example, from grain boundary triple points, and transgranular fracture is initiated in these bands. A more detailed discussion of the deformation bands will be given later.

(2) *(α + β) ST plus α-aged microstructures*

These microstructures are commercially the most interesting, since they exhibit the best combinations of mechanical properties (Figure 3).[4,9] It appears useful to start the discussion using a fixed microstructure with a constant yield stress, for example, with 10 pct α_p aged to 1250 MPa. Deformation studies have shown that, at the inception of plastic

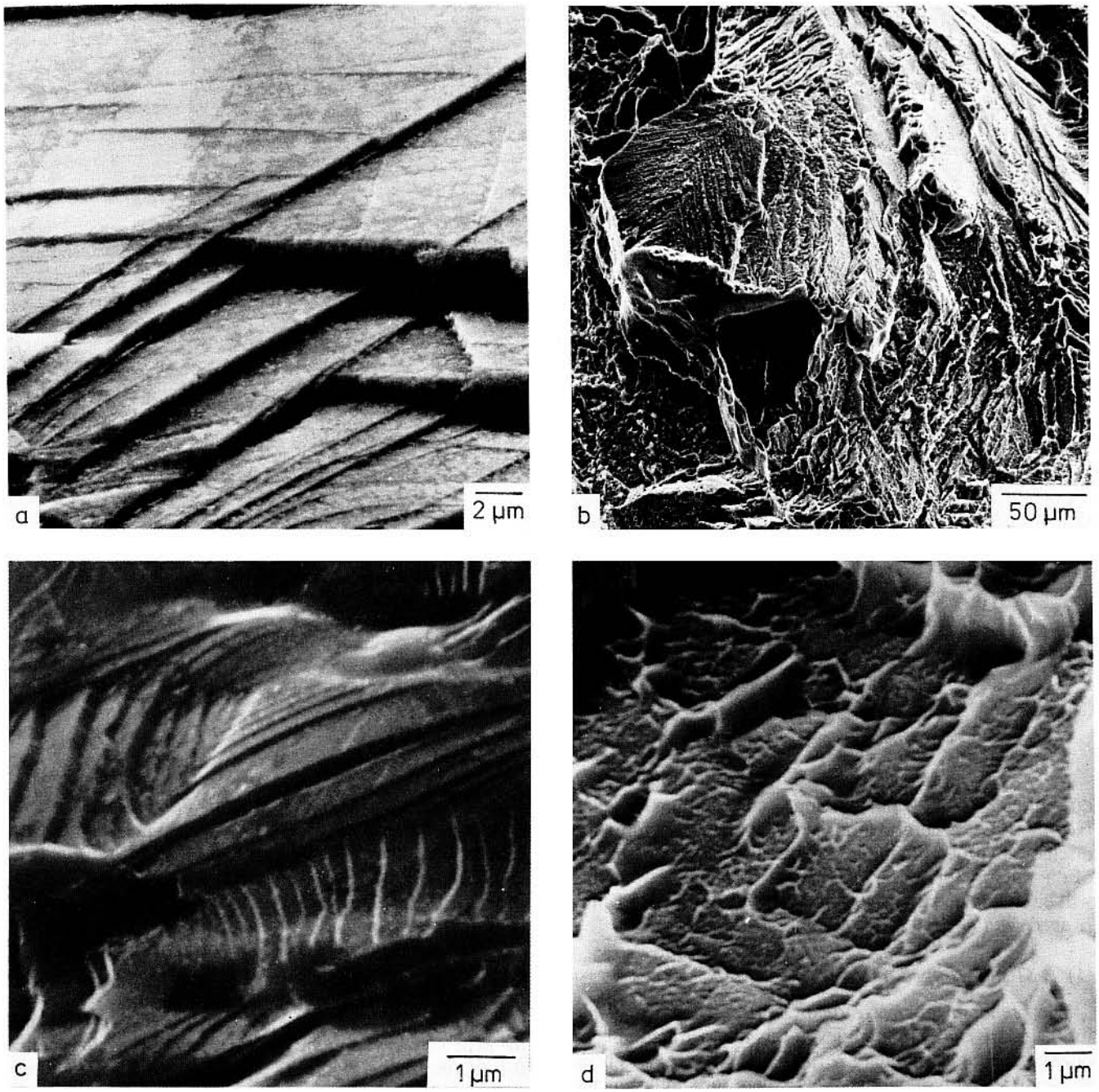

Fig. 13—Plastic deformation and fracture in 2 different ω-aged microstructures, SEM. (a, b) β-ST + ω-aged, grain size ~150 μm, $\varepsilon_F = 0$. (c, d) $(\alpha + \beta)$ ST + ω-aged, 30 pct α_p, grain size ~10 μm, $\varepsilon_F = 0.31$.

deformation, the plastic strain is homogeneously distributed throughout the microstructure, but that at higher strains the onset of strain localization occurs. For high volume fractions of small α_s, the strain localization can become extreme and can lead to macroscopic brittleness (Figure 8). Although the microscopic results are not totally conclusive, it is possible to provide some insight into the nature of the observed deformation bands and the role of these bands in the overall fracture process. At low plastic strains the α- and β-phase strain harden separately, and the α-phase apparently acts as a barrier to slip propagation. With increasing plastic strain, the independent strain hardening of the two phases becomes more difficult because of incompatibility brought about by differences in the strain hardening behavior of the two phases. The details of the strain hardening of these two ductile phases are not totally clear yet, but two recent studies have shown that the small α_s-particles exhibit a high strength which is either produced by a rapid strain hardening of the basicly soft α-phase especially for small dimensions (Hamajima, Lütjering, Weissmann[20]) or by a high initial dislocation density induced by transformation strains (Young, Levine, Margolin[21]). This causes a microstructure condition similar to a dispersion strengthened system except that the α-particles despite their high strength are

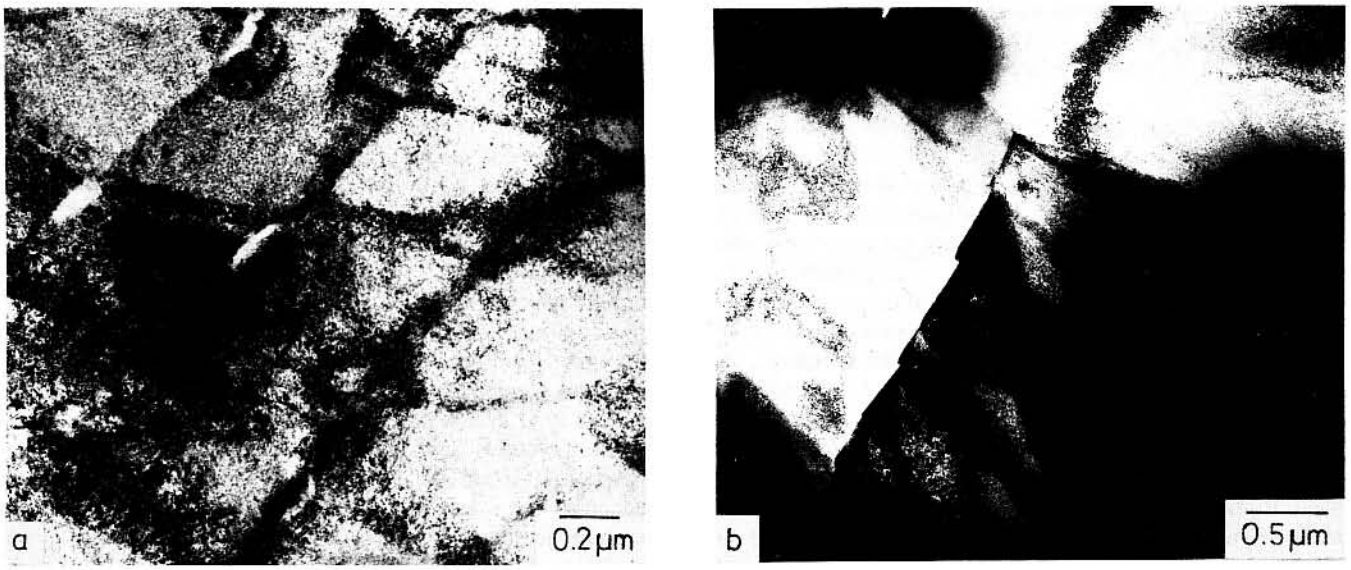

Fig. 14—Microscopic deformation in an (α + β) ST plus ω-aged microstructure, 30 pct α_p, recrystallized, ε_F = 0.31, TEM. (*a*) Intersecting slip bands, (*b*) offsets at grain boundaries caused by intense slip bands.

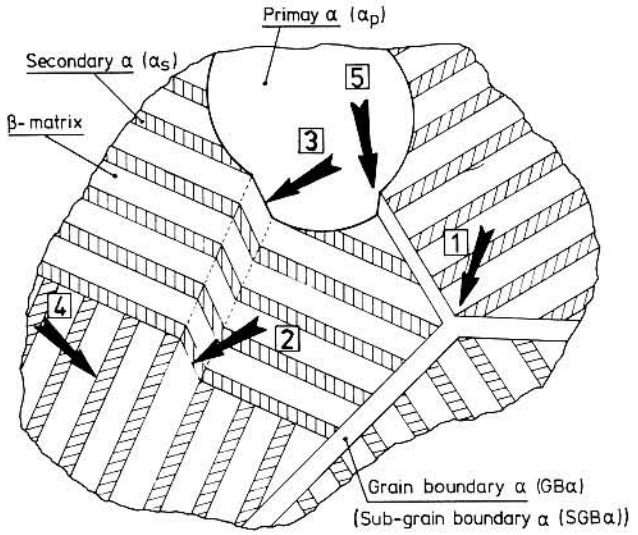

Fig. 15—Schematic illustration of stress or strain concentrations acting as possible void nucleation sites.

still capable of deforming plastically. As a result and in contrast to rigid dispersoids it is possible to deform further the α-phase plastically which defers nucleation of voids at the α-β interface until higher strains are reached. This further deformation occurs as localized deformation bands. The bands can develop in two ways as illustrated in Figure 15 (arrow 2): (1) slip can pass through the α-β interfaces as has been observed already for other Ti-alloys.[21,22] This reaction is likely since, according to the Burgers orientation relationship, the α- and β-phase have several common slip systems and Burgers vectors of comparable magnitude. This transition of slip from β to α should happen at sites with high local stress or strain concentrations. Such a site is, for example, at the boundary of two α_s-β colonies as is indicated by arrow 2 in Figure 15. The local stresses at the colony boundary are highest if (1) the slip occurs in the maximum shear stress direction and (2) if the α_s-plates lie parallel to the slip direction, since in that case the slip length has its maximum value (~colony size). The second possible explanation of the observed slip phenomenon is based on the assumption that slip does not pass through the α_s-β interface, but that instead the local stress concentrations at the interface may induce slip in the α-phase leading to a shearing of this α and of the adjacent β and so on. The favorable sites for the second mechanism are the same as for the first. Both mechanisms could explain the statistical formation of deformation bands at favored sites linking up to microbands at an angle of about 45 deg to the load.

An interesting question arising from the above discussion is if and how the observed slip distribution will influence the fracture process. In this study most of the emphasis has been placed on the crack initiation part of the fracture. Our observations show that crack initiation occurs mainly at primary α particles. This has been found in numerous two phase Ti alloys; however, a clear criterion for void nucleation has not been identified yet. Our results suggest that the voids start at those sites where the deformation bands impinge on the interface between α_p and aged matrix. These sites also correspond to regions of high stress or strain concentrations and lead to offsets in the interface (Figures 11(b), 12(b), 15 (arrow 3)) and to void nucleation there. From this the following conclusions can be drawn: first, the primary α boundaries are important void nucleation sites. Second, however, the aged matrix or secondary α also has a strong effect on the void nucleation process, since it controls the propensity for deformation band formation, and it is these deformation bands which cause void nucleation.

In the above discussion only a fixed microstructure and yield stress (*e.g.*, 10 pct α_p, $\sigma_{0.2}$ = 1250 MPa) were considered. It is now appropriate to consider how changes in the microstructural parameters can influence the strain localization, void nucleation, and the corresponding mechanical properties.

An increase in the volume fraction of the secondary α and a reduction in the α_s particle size leads to an increased

yield stress, a higher strain hardening during plastic deformation, and to a lower ductility (Figure 3).[14] This is accompanied by an increasing propensity for strain localization (Figures 6 and 8).

This observation can be explained by the results of an aforementioned study on a different β-Ti-alloy (Ti-7Mo-7Al),[20] which show that the small α-particles strain harden much more rapidly than the large α-particles. This leads to an increased strain hardening difference between the α- and β-phase and to the formation of deformation bands at lower strains. Increasing the volume fraction of α_s-particles would lead to a more rapid overall strain hardening because the α-particles strain harden much faster than the β-matrix, and again the strain hardening differences which lead to shear band formation would be reached at small macroscopic strains. Taking an increased α_s-dislocation density with decreasing α_s-size[21] would lead to similar tendencies for the band formation. Besides the α_s-size, its plate-like morphology might affect the band formation.[14] Based on the mechanism shown in Figure 15, one would expect that for an increasing plate length the slip length within a colony increases, which in turn raises the stress concentration at the interface to the next colony and leads to band formation at lower strains. This model would explain the unexpected ductility drop during overaging of the microstructure with 10 pct α_p and the high aspect ratio α_s, since the only microstructural change observed was an increased plate length and possibly thickness.

Changing the primary α condition also affects the deformation and fracture, as will be shown by two examples. First, changing the morphology of the primary α from globular to elongated leads to a lower ductility at comparable yield stresses (Table II). A possible explanation is the decreased planar interparticle spacing[23] for the elongated compared to the globular α_p causing a higher void density when the deformation bands cut through them. Changing the volume fraction of α_p has two effects. First, it also reduces the α_p-spacing leading to a higher void density. In addition, when comparing two microstructures with a constant yield stress but different α_p volume fractions, the increased volume fraction of soft primary α does not contribute to the strength and must be offset by a higher matrix strength in order to reach the same macroscopic yield stress. Such a matrix has been shown to favor earlier formation of the deformation bands and to fracture at lower strains (see Figure 3).

The discussion up to this point has focused mainly on the deformation bands and the void formation associated with these bands because this appears to be the dominant process. In addition, however, further types of void nucleation have been observed. For example, voids have been seen at the sites where subgrain boundaries impinge on the α_p-particles (Figures 12(b) and 15 (arrow 5)). Void formation at such sites is likely because there will be high local stresses or steep strain gradients in the regions where the aged matrix, the soft α_p, and the subgrain α interact. Finally, a few instances of crack initiation have also been observed within the aged matrix, especially for microstructures with very long α_s-plate dimensions (Figures 12(c) and 15 (arrow 4)).

Based on this discussion some more general conclusions can be made: deformation and fracture depend very sensitively on the qualitative microstructure type and on the yield stress (consider, for example, the 10 pct α_p microstructure aged to $\sigma_{0.2}$ = 1250 MPa). In addition, it appears that the relative quantitative dimensions and volume fractions of the different types of α also play an important role in initiating voids. The general controlling parameters seem to be local stress or strain concentrations which can occur at several sites within the microstructure (α_p-β interface, α_s-β interface, α_p-subgrain boundary interface, grain boundary α-film). Moreover, which site becomes active for void nucleation or how the different possible sites work in a combination appears to be sensitively controlled by the quantitative mixture of α-types, volume fractions, and morphologies. For example, deformation bands are the dominant void nucleation site at higher yield stresses while at lower yield stresses the interfaces between α_p and SGBα and/or aged matrix can act as void nucleation sites.

For a complete correlation between microscopic and macroscopic fracture the crack growth has to be taken into account. Although in this study this has not been done systematically, it has been observed that, especially in the high strength conditions, voids were not visible even at high magnifications (10,000 times) until very shortly before fracture. This suggests that the contribution of the crack growth process to the ductility in those conditions is not very marked and that it is mainly controlled by the strain hardening and void nucleation.

(3) *ω-aged microstructures*

During deformation of the ω-aged conditions the ω-particles are sheared by moving dislocations (Figures 14 and 15). Intense slip bands (dislocation pile-ups) form; they create high stress concentrations at slip barriers like grain boundaries and primary α-particles. This can lead to crack nucleation at these sites at very low macroscopic strains. The extent to which these stress concentrations develop is influenced by the yield stress increase due to particle hardening as well as by the slip length (grain size and/or α_p-spacing).[24] Both of these factors affect ductility. These correlations permit mechanical properties to be explained. The ductility increases continuously if one compares a large grain ($\sim$150 μm) in the β-ST condition (ε_F = 0), with the (α + β) ST condition with 30 pct α_p and a substructure (ε_F = 0.02) and with the (α + β) ST condition with the same amount of α_p but very small recrystallized grains ($\sim$10 μm diameter) (ε_F = 0.31). A comparison of the three microstructures also shows that neither the subgrain boundaries nor the α_p are effective barriers for slip bands compared to a grain refinement. An improvement of the yield stress-ductility combination would be reached by further reducing the grain size and also by reducing the primary α volume fraction. The latter suggestion is made since the soft primary α leads to early accumulation of plastic strain, and in order to reach a certain macroscopic yield stress the matrix has to be more extensively ω-strengthened than in a structure without the α_p. This, in turn, lowers the ductility.

VI. CONCLUSIONS

In Ti-10-2-3 a variety of microstructures has been studied. They were established by a combination of forging, solution treating, and subsequent aging and were characterized by different types of α (α_p, α_s, SGBα, GBα), with different

volume fractions and morphologies. The results can be summarized as follows:

1. For different microstructures a wide range of yield stresses can be reached varying from about 900 MPa to 1450 MPa.
2. The ductility depends strongly on the microstructure and the yield stress. A yield stress increase reduces the ductility for a fixed microstructure; the sensitivity $\Delta RA/\Delta\sigma_{0.2}$ showed values up to 22 pct per 100 MPa.

   For the $(\alpha + \beta)$ ST plus α-aged microstructures increasing the α_p volume fraction as well as changing from globular to elongated α_p reduces the ductility at comparable yield stresses. The β-ST plus α-aged conditions have lower ductilities than the $(\alpha + \beta)$ ST plus α-aged conditions. For a ω-aged microstructure (30 pct α_p) a transition from macroscopic brittleness to a marked ductility ($\varepsilon_F = 0.31$ at $\sigma_{0.2} = 1250$ MPa) has been observed, when the grain size is reduced from 150 μm to 10 μm. A detailed microscopical study of deformation and fracture has revealed a variety of slip and fracture modes. For the β-ST plus α-aged microstructures the grain boundary α film is the dominant parameter for fracture since the plastic strain is localized in this small volume leading to premature fracture and to low ductilities. In the $(\alpha + \beta)$ ST plus α-aged conditions the onset of fracture depends sensitively and in a complex way on the combination of factors including the types of $\alpha(\alpha_p, \alpha_s, \text{SGB}\alpha, \text{GB}\alpha)$, their morphologies, and volume fraction.

It is concluded that several possible sites with stress or strain concentrations exist in the microstructure, and which are active for void nucleation depends on the above combinations. With increasing yield stresses (high volume fraction of α_s, *e.g.*), a pronounced tendency for matrix strain localization has been observed. This leads to crack nucleation at increasingly lower strains at α_p particles, which are cut by the localized deformation bands. An explanation is given based on different rates of strain hardening in the α_s and β-phase which lead to high stress concentrations at the α_s-β interfaces at a colony boundary and to a transition of slip through the interface (Figure 15). Voids also have been observed at the interface between α_s and β, especially at lower yield stresses as well as at the sites where subboundaries impinge on the α_p-particles. Both observations are explained by increased stress concentrations at the particular sites.

In the ω-aged conditions during plastic deformation the coherent ω-particles are sheared by moving dislocations, which leads to planar slip with high stress concentrations at the slip barriers like grain boundaries and interfaces between α_p and ω-aged matrix. Reducing the slip length by a decreasing grain size can improve the ductility considerably.

REFERENCES

1. E. Bohanek: *Titanium Science and Technology*, R. I. Jaffee and H. M. Burte, eds., Plenum Press, New York, NY, 1973, vol. 3, p. 1983.
2. F. H. Froes, J. C. Chesnutt, C. G. Rhodes, and J. C. Williams: ASTM STP 651, *Toughness and Fracture Behavior of Titanium*, 1978, p. 115.
3. F. H. Froes, R. F. Malone, V. C. Peterson, C. G. Rhodes, J. C. Chesnutt, and J. C. Williams: AFML-TR-75-4, Air Force Materials Laboratory, Dayton, OH, 1975, vols. I and II.
4. J. C. Williams, F. H. Froes, J. C. Chesnutt, C. G. Rhodes, and R. G. Berryman: ASTM STP 651, *Toughness and Fracture Behavior of Titanium*, 1978, p. 64.
5. H. W. Rosenberg: Joint Conference: Forging and Properties of Aerospace Materials, University of Leeds, Leeds, England, January 1977.
6. E. Bohanek: Technical Report No. 55, Titanium Metals Corporation of America, May 1972.
7. C. C. Chen and C. P. Gure: Report RD74-120, Wyman-Gordon Company, North Grafton, MA, November 1975.
8. C. C. Chen: Report RD-75-118, Wyman-Gordon Company, North Grafton, MA, November 1975.
9. R. R. Boyer: *Journal of Metals*, March 1980, vol. 32, p. 61.
10. C. C. Chen and R. R. Boyer: *Journal of Metals*, July 1979, vol. 31, p. 33.
11. G. Lenning: Report No. RD 012, TIMET, March 1976.
12. I. A. Martorell: AFML-TR-78-114, Air Force Materials Laboratory, Dayton, OH, 1978.
13. E. L. Herman, J. Kozol, and A. R. Troiano: *Trans. ASM*, 1958, vol. 50, p. 418.
14. T. W. Duerig, G. T. Terlinde, and J. C. Williams: *Metall. Trans. A*, 1980, vol. 11A, p. 1987.
15. A. Gysler, G. Terlinde, and G. Luetjering: Proc. 3rd Int. Conf. on Titanium, Moscow, USSR, J. C. Williams and A. F. Belov, eds., Plenum Press, New York, NY, 1981, p. 1919.
16. T. W. Duerig and J. C. Williams: Carnegie-Mellon University, Pittsburgh, PA, unpublished research, 1981.
17. G. Terlinde and J. C. Williams: Carnegie-Mellon University, Pittsburgh, PA, unpublished research, 1980.
18. M. Peters and G. Luetjering: *Zeitschrift f. Metallkunde*, 1976, vol. 67, p. 811.
19. M. Gräf: *Metall.*, 1978, vol. 32, p. 563.
20. T. Hamajima, G. Luetjering, and S. Weissmann: *Metall. Trans.*, 1973, vol. 4, p. 847.
21. M. Young, E. Levine, and H. Margolin: *Metall. Trans. A*, 1979, vol. 10A, p. 359.
22. K. S. Chan, C. C. Wojcik, and D. A. Koss: *Metall. Trans. A*, 1981, vol. 12A, p. 1899.
23. P. P. Bonsel and A. J. Ardell: *Metallography*, 1972, vol. 5, pp. 97-111.
24. G. Terlinde and G. Luetjering: *Metall. Trans. A*, 1982, vol. 13A, p. 1283.
25. H. Margolin and Y. Mahajan: *Metall. Trans. A*, 1978, vol. 9A, p. 781.